Quasi one-dimensional light beam generated by a graded-index microsphere

Soon-Cheol Kong,[1,*] Allen Taflove,[1] and Vadim Backman[2]

[1] *Department of Electrical Engineering and Computer Science, Northwestern University, Evanston, IL 60208, USA*
[2]*Department of Biomedical Engineering, Northwestern University, Evanston, IL 60208, USA*
[*]*Corresponding author: sch@northwestern.edu*

Abstract: An optically illuminated micron-scale dielectric sphere can generate a photonic nanojet – a nonresonant propagating beam phenomenon of high amplitude, narrow waist, and substantial sensitivity to the presence of nanometer-scale particles and geometric features located within the beam. Via three-dimensional finite-difference time-domain computational electrodynamics modeling of illuminated graded-index microspheres, we have found that the useful length of a photonic nanojet can be increased by an order-of-magnitude to approximately 20 wavelengths. This is effectively a quasi one-dimensional light beam which may be useful for optical detection of natural or artificially introduced nanostructures deeply embedded within biological cells. Of particular interest in this regard is a potential application to visible-light detection of nanometer-scale anomalies within biological cells indicative of early-stage cancer.

OCIS codes: (210.0210) Optical data storage; (230.3990) Micro-optical devices; (290.1350) Backscattering.

References and links

1. Z. Chen, A. Taflove, and V. Backman, "Photonic nanojet enhancement of backscattering of light by nanoparticles: A potential novel visible-light ultramicroscopy technique," Opt. Express **12**, 1214-1220 (2004).
2. X. Li, Z. Chen, A. Taflove, and V. Backman, "Optical analysis of nanoparticles via enhanced backscattering facilitated by 3-D photonic nanojets," Opt. Express **13**, 526-533 (2005).
3. S. Lecler, Y. Takakura, and P. Meyrueis, "Properties of a three-dimensional photonic jet," Opt. Lett. **30**, 2641-2643 (2005).
4. A. V. Itagi and W. A. Challener, "Optics of photonic nanojets," J. Opt. Soc. Am. A **22**, 2847-2858 (2005).
5. Z. G. Chen, X. Li, A. Taflove, and V. Backman, "Superenhanced backscattering of light by nanoparticles," Opt. Lett. **31**, 196-198 (2006).
6. A. Heifetz, K. Huang, A. V. Sahakian, X. Li, A. Taflove, and V. Backman, "Experimental confirmation of backscattering enhancement induced by a photonic jet," Appl. Phys. Lett. **89**, 221118 (2006).
7. A. M. Kapitonov and V. N. Astratov, "Observation of nanojet-induced modes with small propagation losses in chains of coupled spherical cavities," Opt. Lett. **32**, 409-411 (2007).
8. K. J. Yi, H. Wang, Y. F. Lu, and Z. Y. Yang, "Enhanced Raman scattering by self-assembled silica spherical microparticles," J. Appl. Phys. **101**, 063528 (2007).
9. S. Lecler, S. Haacke, N. Lecong, O. Crégut, J.-L. Rehspringer, and C. Hirlimann, "Photonic jet driven non-linear optics: Example of two-photon fluorescence enhancement by dielectric microspheres," Opt. Express **15**, 4935-4942 (2007).
10. W. Wu, A. Katsnelson, O. G. Memis, and H. Mohseni, "A deep sub-wavelength process for the formation of highly uniform arrays of nanoholes and nanopillars," Nanotechnology **18**, 485302 (2007).
11. A. Heifetz, J. J. Simpson, S.-C. Kong, A. Taflove, and V. Backman, "Subdiffraction optical resolution of a gold nanosphere located within the nanojet of a Mie-resonant dielectric microsphere," Opt. Express **15**, 17334-17342 (2007).
12. M. Gerlach, Y. P. Rakovich, and J. F. Donegan, "Nanojets and directional emission in symmetric photonic molecules," Opt. Express **15**, 17343-17350 (2007).

#104866 - $15.00 USD Received 4 Dec 2008; revised 18 Jan 2009; accepted 19 Jan 2009; published 25 Feb 2009

13. P. Ferrand, J. Wenger, A. Devilez, M. Pianta, B. Stout, N. Bonod, E. Popov, and H. Rigneault, "Direct imaging of photonic nanojets," Opt. Express **16**, 6930-6940 (2008).
14. S.-C. Kong, A. V. Sahakian, A. Heifetz, A. Taflove, and V. Backman, "Robust detection of deeply subwavelength pits in simulated optical data-storage disks using photonic jets," Appl. Phys. Lett. **92**, 211102 (2008).
15. S. Yang and V. N. Astrov, "Photonic nanojet-induced modes in chains of size-disordered microspheres with an attenuation of only 0.08 dB per sphere," Appl. Phys. Lett. **92**, 261111 (2008).
16. E. McLeod and C. B. Arnold, "Subwavelength direct-write nanopatterning using optically trapped microspheres," Nat. Nanotech. **3**, 413-417 (2008).
17. Z. Chen, H. Chu, and S. Li, "Optical metrology using a photonic nanojet," U.S. Patent 7,394,535 (2008).
18. X. Cui, D. Erni, and C. Hafner, "Optical forces on metallic nanoparticles induced by a photonic nanojet," Opt. Express **16**, 13560-13568 (2008).
19. S.-C. Kong, A. V. Sahakian, A. Taflove, and V. Backman, "Photonic nanojet-enabled optical data storage," Opt. Express **16**, 13713-13719 (2008).
20. A. Devilez, B. Stout, N. Bonod, and E. Popov, "Spectral analysis of three-dimensional photonic jets," Opt. Express **16**, 14200-14212 (2008).
21. A. Taflove, and S. C. Hagness, *Computational Electrodynamics: The Finite-Difference Time-Domain Method*, 3rd ed. (Artech, Boston, MA 2005).
22. S.-C. Kong, J. J. Simpson, and V. Backman, "ADE-FDTD scattered-field formulation for dispersive materials," IEEE Microwave Wireless Comp. Lett. **18**, 4-6 (2008).
23. E. Prodan, C. Radloff, N. J. Halas, and P. Nordlander, "A hybridization model for the plasmon response of complex nanostructures," Science **302**, 419-422 (2003).
24. J. F. Poco, and L. W. Hrubesh, "Method of producing optical quality glass having a selected refractive index," U.S. Patent 6,158,244, (2008).
25. O. V. Mazurin, M. V. Streltsina, and T. P. Shvaiko-Shavaikovskaya, *Handbook of Glass Data* (Elsevier, Amsterdam, 1993).
26. M. A. Ordal, L. L. Long, R. J. Bell, S. E. Bell, R. R. Bell, R. W. Alexander, Jr., and C. A. Ward, "Optical properties of the metals Al, Co, Cu, Au, Fe, Pb, Ni, Pd, Pt, Ag, Ti, and W in the infrared and far infrared," Appl. Opt. **22**, 1099 (1983).
27. C. A. Balanis, *Antenna Theory: Analysis and Design* (John Wiley & Sons, New York, 1982).
28. H. Subramanian, P. Pradhan, Y. Liu, I. Capoglu, X. Li, J. Rogers, A. Heifetz, D. Kunte, H. K. Roy, A. Taflove, and V. Backman, "Optical methodology for detecting histologically unapparent nanoscale consequences of genetic alterations in biological cells," Proc. National Acad. Sci. **105**, 20124-20129 (2008).

1. Introduction

The photonic nanojet (PNJ) is a subwavelength (sub-λ) waist, high-intensity light beam that can propagate over a distance longer than λ after emerging from the shadow-side surface of an illuminated lossless dielectric microcylinder or microsphere of diameter larger than λ [1–20]. The PNJ appears for a wide range of diameters of the microcylinder or microsphere if the refractive index contrast relative to the background is less than about 2:1 [1].

A key characteristic of the PNJ is that inserting within it a nanoparticle of diameter d_v perturbs the far-field backscattered power of the illuminated microsphere by an amount that varies as d_v^3 for a fixed λ. This perturbation is much slower than the d_v^6 dependence of Rayleigh scattering for the same nanoparticle. It leads to a situation where the backscattered power of a 3-μm polystyrene microsphere more than doubles if a 30-nm gold nanoparticle is inserted into the PNJ emerging from the microsphere, despite the nanoparticle having only 1/10,000th the cross-section area of the microsphere [2]. In effect, the PNJ strongly projects the presence of the nanoparticle to the far field.

Potentially important applications of PNJs include detecting/sizing [2] and manipulating [18] nanoscale objects, maskless subwavelength-resolution direct-write nanopatterning and nanolithography [10, 16], broadband low-loss waveguiding [7, 15], and ultrahigh-density optical data storage [14, 19].

#104866 - $15.00 USD Received 4 Dec 2008; revised 18 Jan 2009; accepted 19 Jan 2009; published 25 Feb 2009

We are interested in applying the far-field projection property of the PNJ to achieve high spatial resolution detection of nanostructures deeply embedded within biological cells, including both intrinsic nanostructures and artificially introduced nanoparticles. However, in pursuit of this goal, we have been limited by the short length of the PNJ (only in the order of λ), which allows it to interact with only near-surface features of the cell.

Consequently, we have conducted three-dimensional finite-difference time-domain (FDTD) computational electrodynamics modeling [21, 22] to investigate how a PNJ's length might be increased while retaining its far-field projection property. In the approach reported in this paper, we consider grading the refractive index of the plane-wave-illuminated, PNJ-generating microsphere such that the refractive index decreases linearly in the radial direction.

2. Model of the graded-index microsphere

We define the refractive index contrast (relative to the background medium) of the graded-index microsphere as

$$n(r) = n_{\max} - \frac{(n_{\max} - 1)}{a} r \tag{1}$$

Here, a is the radius of the microsphere and r is the distance from the microsphere's center. In the present study, n_{max} is set to 2. Thus, the refractive index contrast has a maximum value of 2 at the center of the microsphere, and decreases linearly in the radial direction to a minimum value of 1 at the microsphere surface.

In the present work, we consider refractive index gradings realized with 5, 10, or 100 distinct concentric shells. Fabrication of such microspheres should be possible using nanoshell techniques [23]. The controlled synthesis of materials with refractive indices in the range 1.05 to 1.28 has been reported [24] by varying the composition and porosity of silica glass. Higher refractive indices from 1.4 to 1.9 can be obtained from various available glasses [25].

3. Field distribution and power flow

Figure 1(a) visualizes the FDTD-computed scattered electric-field (*E*-field) envelope, normalized relative to the incident plane-wave amplitude, for a homogeneous 2-μm diameter polystyrene microsphere ($n = 1.59$) illuminated in free space at $\lambda = 400\,\text{nm}$. This visualization is in the plane cutting through the center of the microsphere that is defined by the incident *x*-directed *E*-field vector and *z*-directed Poynting vector. Figure 1(b) is the corresponding visualization for a homogeneous 2-μm diameter silica microsphere ($n = 1.43$). In each of these cases, a standing-wave pattern is observed within the microsphere.

Figure 1(c) visualizes the scattered *E*-field envelope for a graded-index microsphere of the same diameter as specified in Eq. (1), wherein the grading is realized with 100 concentric shells, each 10 nm thick. In this case, we see no standing waves within the microsphere, but instead a C-shaped pattern that connects to sidelobes adjacent to the PNJ. Comparing Figs. 1(a), 1(b), and 1(c), we see that the graded-index microsphere generates a significantly elongated PNJ in the *z*-direction.

Figures 1(d) and 1(e) are *E*-field visualizations corresponding to Fig. 1(c) wherein the refractive index grading is realized with ten 100-nm-thick shells and five 200-nm-thick shells, respectively. We see that the field distributions in Figs. 1(d) and 1(e) are qualitatively similar to the 100-shell case of Fig. 1(c), differing primarily by having a narrower PNJ beamwidth. Thus, we conclude that an elongated PNJ can be realized with a graded-index microsphere having a relatively small number of concentric shells, thereby being more practical from a manufacturing standpoint.

#104866 - $15.00 USD Received 4 Dec 2008; revised 18 Jan 2009; accepted 19 Jan 2009; published 25 Feb 2009

(a) Homogeneous polystyrene, $n = 1.59$.

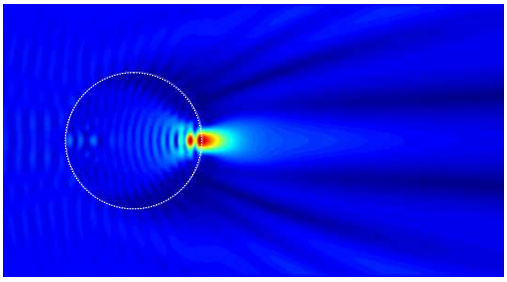

(b) Homogeneous silica, $n = 1.43$.

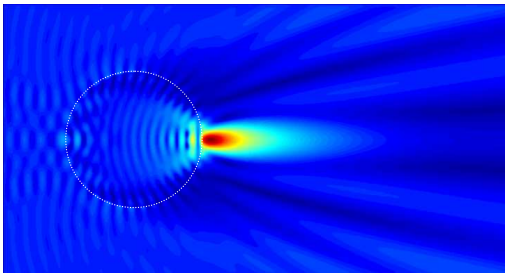

(c) Graded-index dielectric, maximum index $n = 2$ at the center decreasing linearly to $n = 1$ at the surface; grading realized with 100 concentric shells each 10 nm thick.

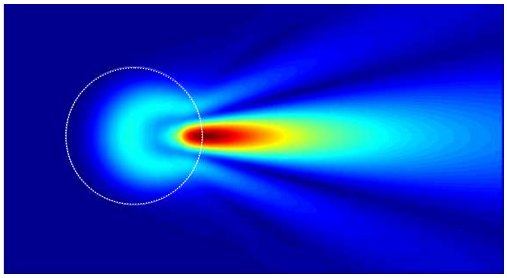

(d) As in (c), but grading realized with ten 100-nm-thick shells.

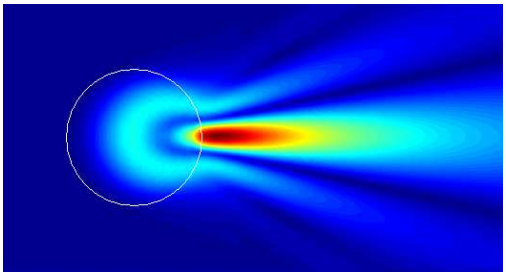

(e) As in (c), but grading realized with five 200-nm-thick shells.

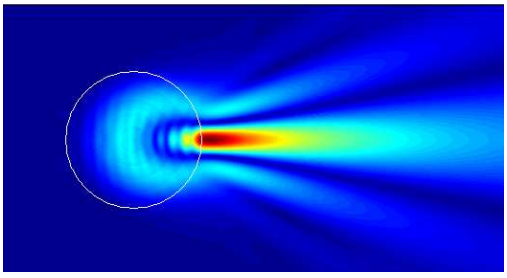

Fig. 1. Visualizations of the FDTD-computed scattered electric field for several 2 μm diameter dielectric microspheres for a 400 nm incident wavelength. Each panel spans 4 μm in the vertical (x) direction × 8 μm in the horizontal (z) direction).

#104866 - $15.00 USD Received 4 Dec 2008; revised 18 Jan 2009; accepted 19 Jan 2009; published 25 Feb 2009

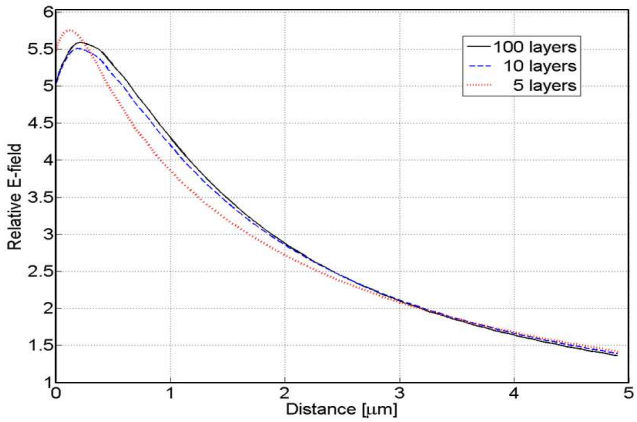

Fig. 2. FDTD-computed normalized optical electric field vs. distance from the microsphere shadow-side surface along the *z*-axis for the cases of Figs. 1(c), 1(d), and 1(e).

Figure 2 shows little difference between the cases of Figs. 1(c), 1(d), and 1(e) for the fall-off of the normalized *E*-field with distance from the microsphere's shadow-side surface along the *z*-axis. Figures 3(a) and 3(b) are arrow depictions of the time-averaged Poynting vector in the 3-D electromagnetic field corresponding to Figs. 1(a) and 1(c). Comparing Figs. 3(a) and 3(b), we see that power flow within the graded-index microsphere is directed to its shadow side (and beyond into the PNJ) more smoothly in space, with greater amplitude, and with smaller transverse components than for the homogeneous polystyrene microsphere.

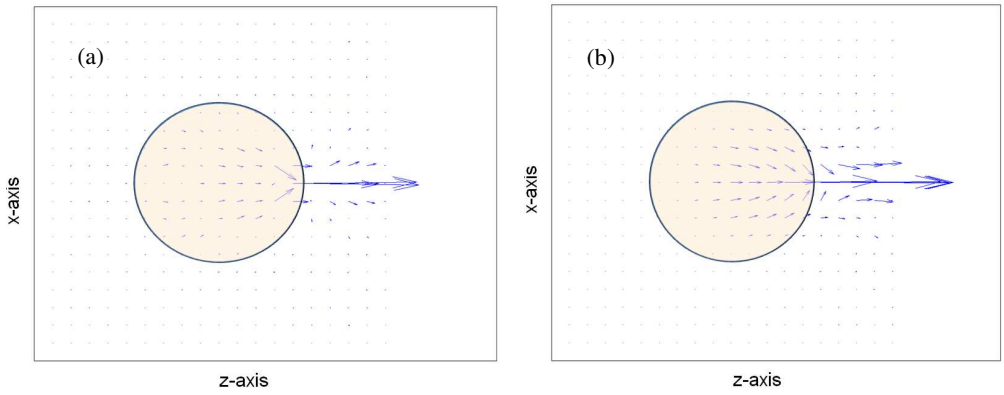

Fig. 3. Arrow-plot visualization of the FDTD-computed electromagnetic power flow in the *x*-*z* plane. (a) Homogeneous polystyrene microsphere ($n=1.59$) of Fig. 1(a). (b) 100-shell graded-index microsphere of Fig. 1(c).

Figure 4 graphs the normalized intensity along the *z*-axis within the center of the PNJ as a function of distance from the microsphere's shadow-side surface for the polystyrene microsphere of Fig. 1(a), the silica microsphere of Fig. 1(b), and the 100-shell graded-index microsphere of Fig. 1(c). We see that the PNJ intensity for the graded-index microsphere decreases more slowly with distance, especially beyond 2 μm (5λ). To quantify this, we define the PNJ beam length L_{beam} as the distance from the microsphere's shadow-side surface to the point along the *z*-axis where the PNJ intensity drops to twice the incident. Here, the calculated L_{beam} values are 1.87 μm (4.675λ) for the polystyrene microsphere, 2.04 μm (5.1λ) for the silica microsphere, and 4.72 μm (11.8λ) for the graded-index microsphere.

#104866 - $15.00 USD Received 4 Dec 2008; revised 18 Jan 2009; accepted 19 Jan 2009; published 25 Feb 2009

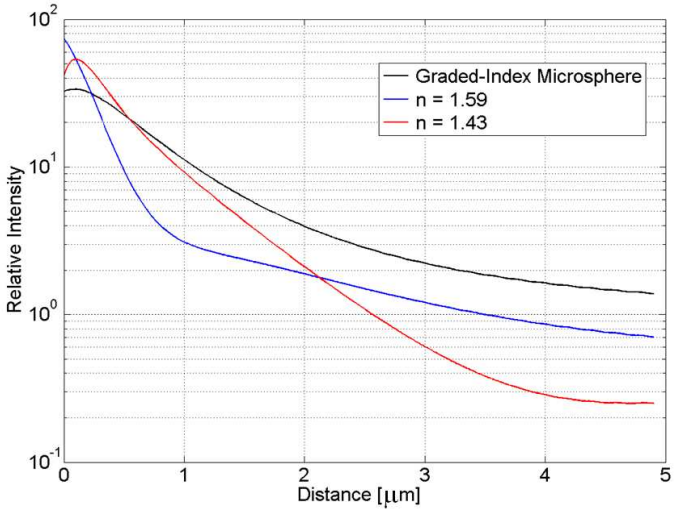

Fig. 4. FDTD-computed photonic nanojet intensity relative to the incident plane wave vs. distance from the microsphere's shadow-side surface along the z-axis. Illumination wavelength = 400 nm. Three cases: homogeneous n = 1.59 polystyrene microsphere of Fig. 1(a), homogeneous n = 1.43 silica microsphere of Fig. 1(b), and 100-shell graded-index microsphere of Fig. 1(c).

4. Backscattering

Figure 5 compares the FDTD-computed backscattered power vs. wavelength near $\lambda = 400$ nm for the isolated homogeneous n = 1.59 polystyrene microsphere of Fig. 1(a), the isolated homogeneous n = 1.43 silica microsphere of Fig. 1(b), and the isolated 100-shell graded-index microsphere of Fig. 1(c). In this figure, the data are plotted with a resolution of 0.5 nm.

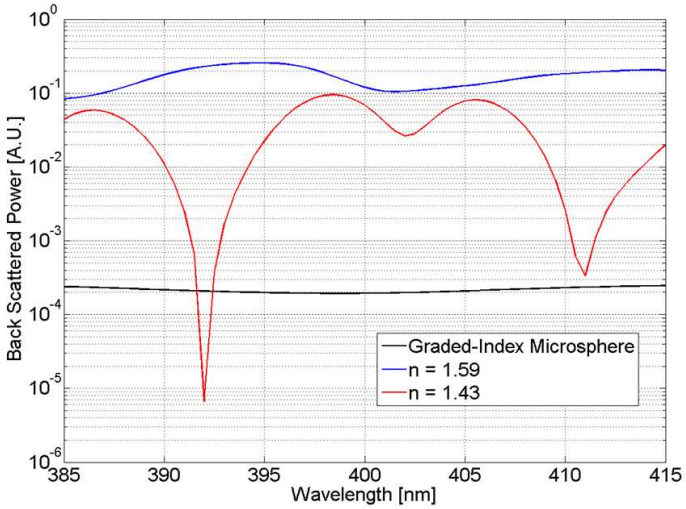

Fig. 5. FDTD-computed backscattered power of an isolated 2-μm diameter microsphere vs. wavelength. Three cases: homogeneous n = 1.59 polystyrene microsphere of Fig. 1(a), homogeneous n = 1.43 silica microsphere of Fig. 1(b), and 100-shell graded-index microsphere of Fig. 1(c).

#104866 - $15.00 USD Received 4 Dec 2008; revised 18 Jan 2009; accepted 19 Jan 2009; published 25 Feb 2009

From Fig. 5, we see that the graded-index microsphere has a much smaller backscattering than the two homogeneous microspheres; for example, ~30 dB lower than the polystyrene microsphere at $\lambda = 400$ nm. The decrease in backscattering results from the enhanced +z-directed transmission illustrated in Fig. 1(c) and Fig. 3. Furthermore, the backscattering of the graded-index microsphere varies little with operating wavelength, implying the possibility of broadband operation with little impact by resonant modes.

Previous studies [1, 2, 6] have shown that inserting a nanoparticle of diameter d_v within a PNJ perturbs the far-field backscattered power of an illuminated homogeneous dielectric microsphere by an amount that varies as d_v^3 for a fixed λ. Here, the microsphere's backscattering perturbation ΔI_μ and the nanoparticle's effective backscattering enhancement factor EF_v are defined as:

$$\Delta I_\mu = \frac{\left| I_{\mu+v} - I_\mu \right|}{I_\mu} \tag{2}$$

$$EF_v = \frac{\left| I_{\mu+v} - I_\mu \right|}{I_v} \tag{3}$$

where I_μ is the backscattering intensity of the isolated microsphere, I_v is the backscattering intensity of the isolated nanoparticle, and $I_{\mu+v}$ is the backscattering intensity of the microsphere upon insertion of a nanoparticle within the PNJ generated by the microsphere. Thus, ΔI_μ represents the measurement dynamic range required to detect the nanoparticle. As stated earlier, the d_v^3 dependence of ΔI_μ for a fixed λ is much slower than the d_v^6 dependence of Rayleigh scattering for the same nanoparticle, if isolated. This leads to a situation where insertion of a nanoparticle within the PNJ generated by the microsphere can markedly impact the microsphere's backscattered power, especially for small-size nanoparticles. In effect, the PNJ strongly projects the presence of the nanoparticle to the far field.

We now consider the FDTD-computed backscattering perturbations for the homogeneous $n = 1.59$ polystyrene microsphere of Fig. 1(a), the homogeneous $n = 1.43$ silica microsphere of Fig. 1(b), and the 100-shell graded-index microsphere of Fig. 1(c). For each of these cases, Fig. 6(a) compares the backscattering perturbation ΔI_μ at $\lambda = 400$ nm as a function of the distance between the shadow-side surface of the microsphere and the center of a 100-nm diameter gold nanoparticle inserted on the longitudinal axis of the nanojet. In order to model the Drude dispersion property of the gold permittivity at optical wavelengths, we used reported values of plasma angular frequency and collision frequency [26].

From Fig. 6(a), we see that at a gold nanoparticle distance of 100 – 200 nm from the microsphere, the normalized backscattering intensity perturbation ΔI_μ for the 100-shell graded-index microsphere is approximately 2000. This is much greater than the 4 – 10 value for the two homogeneous dielectric microspheres. Furthermore, while ΔI_μ for the homogeneous microspheres drops quickly below 1 (i.e., a 100% perturbation) for microsphere-nanoparticle separation distances greater than 500 nm (~1λ), ΔI_μ of the graded-index microsphere remains above 2 (i.e., a 200% perturbation) for separation distances up to at least 8 μm (20λ). This distance regime corresponds to the radiating near-field (Fresnel) region which lies between the reactive near-field region and far-field (Fraunhofer) region [27]. It is of sufficient span to allow probing deeply for scattering nanostructures within a wide variety of individual biological cells.

#104866 - $15.00 USD Received 4 Dec 2008; revised 18 Jan 2009; accepted 19 Jan 2009; published 25 Feb 2009

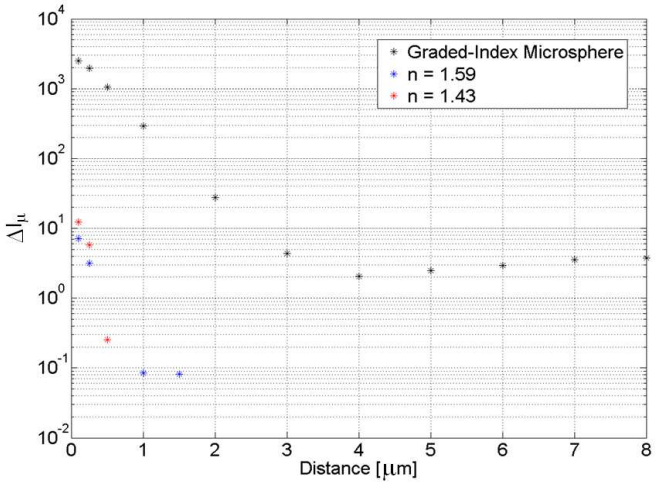

(a)

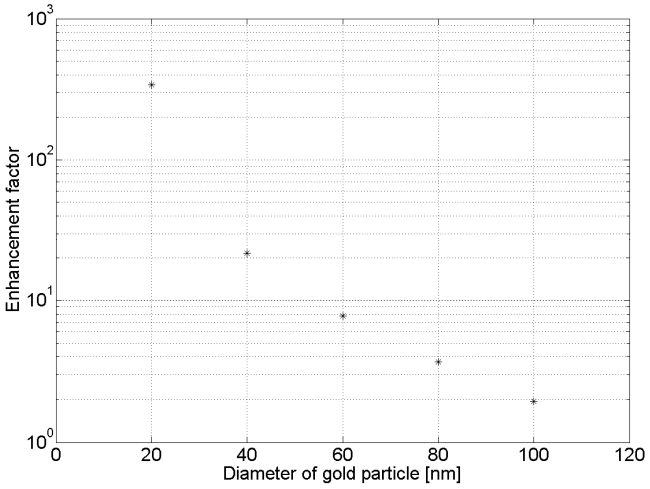

(b)

Fig. 6. (a) FDTD-computed backscattering perturbation of the microsphere with a 100-nm gold nanoparticle located on the z-axis. Horizontal scale: distance between the microsphere's shadow-side surface and the center of the gold nanoparticle. Three cases: homogeneous $n=1.59$ polystyrene microsphere of Fig. 1(a), homogeneous $n=1.43$ silica microsphere of Fig. 1(b), and 100-shell graded-index microsphere of Fig. 1(c). (b) FDTD-computed backscattering enhancement factor of a gold nanoparticle located 8 μm (20λ) beyond the shadow-side surface of the graded-index microsphere of Fig. 1(c).

Figure 6(b) graphs the FDTD-calculated backscattering enhancement factor EF_v defined in Eq. (3) for a gold nanoparticle as a function of its diameter. The 100-shell graded-index microsphere of Fig. 1(c) is assumed, with the gold nanoparticle located at the center of the PNJ at a distance of 8 μm (20λ) from the shadow-side surface of the microsphere. These results show greater than 10:1 effective enhancements of the backscattering of nanoparticles having sizes below 50 nm relative to their backscattering if isolated, with enhancements rising above 100:1 for nanoparticles smaller than about 25 nm.

#104866 - $15.00 USD Received 4 Dec 2008; revised 18 Jan 2009; accepted 19 Jan 2009; published 25 Feb 2009

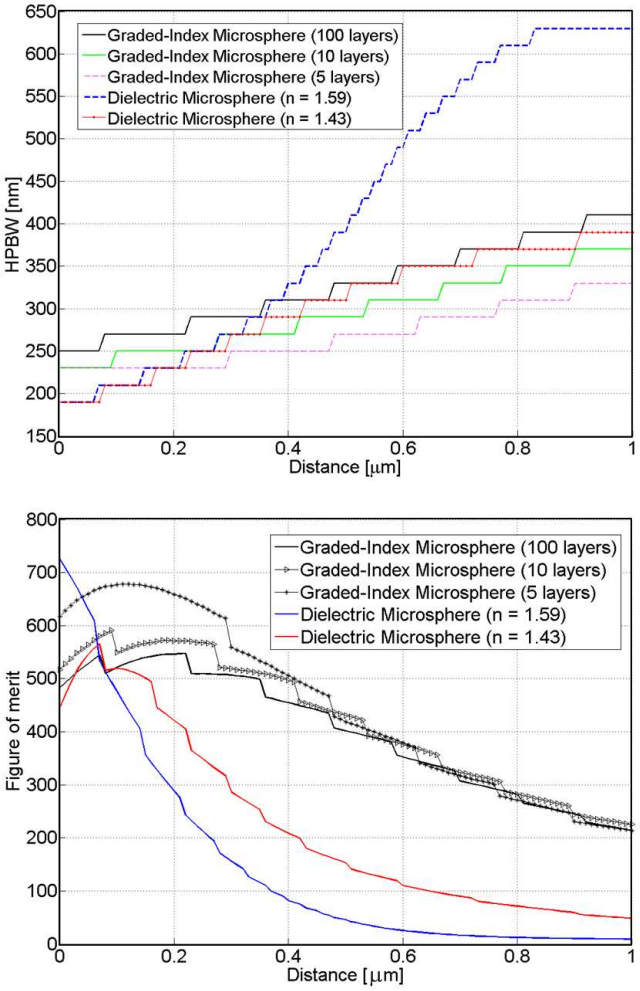

(a)

(b)

Fig. 7. (a) FDTD-computed photonic nanojet half-power beamwidth (HPBW) vs. distance from the microsphere's shadow-side surface along the z-axis. (b) FDTD-computed figure of merit ($E_R \times L_{beam}$/HPBW) vs. distance from the microsphere's shadow-side surface along the z-axis.

Figure 7(a) graphs the FDTD-computed half-power beamwidth (HPBW) of the original and elongated PNJs. Immediately adjacent to the microsphere shadow-side surface, the two homogeneous dielectric microspheres yield narrower HPBWs than the various realizations of the graded-index microsphere. However, the graded-index microsphere has a slower rate of increase of the HPBW with distance from the shadow-side surface. Furthermore, letting E_R denote the local value of the PNJ electric field, we define a local PNJ figure of merit as $E_R \times L_{beam}$/HPBW, which is graphed as a function of distance from the microsphere shadow-side surface in Fig. 7(b). This figure of merit succinctly quantifies the primary characteristics of an intense quasi one-dimensional beam — namely, a large beam length to beamwidth ratio and a high value of electric field. Significantly higher values of this figure of merit are seen for the three realizations of the graded-index microsphere than for the two homogeneous microspheres for distances greater than about 0.2 μm beyond the microsphere.

#104866 - $15.00 USD Received 4 Dec 2008; revised 18 Jan 2009; accepted 19 Jan 2009; published 25 Feb 2009

5. Summary and discussion

In conclusion, our three-dimensional FDTD models show that a graded-index dielectric microsphere can generate a significantly longer photonic nanojet than the corresponding homogeneous microsphere. Furthermore, our results show that a gold nanoparticle located within such a nanojet appreciably perturbs the graded-index microsphere's backscattering even at a distance of 20 wavelengths beyond the microsphere. We have determined that the refractive index grading need not be continuous, but can be as coarse as five individual concentric shells of equal thickness comprised of materials already reported in the literature.

These findings may facilitate the use of visible light for high-resolution optical detection of natural or artificially introduced nanostructures and inhomogeneities deeply embedded within biological cells. In particular, the elongated photonic nanojet satisfies the requirement of a quasi one-dimensional beam for partial-wave spectroscopy [28] detection of nanoscale anomalies within cells indicative of early-stage cancer.

Acknowledgments

The photonic nanojet research by our group was supported in part by NIH Grant R01 EB003682 and NSF Grants CBET-0522639 and CBET-0733868. Jim Spadaro and Nikola Borisov managed and maintained Prof. Backman's computer cluster.

#104866 - $15.00 USD Received 4 Dec 2008; revised 18 Jan 2009; accepted 19 Jan 2009; published 25 Feb 2009